

Quantum-Assisted Machine Learning Models for Enhanced Weather Prediction

Saiyam Sakhuja^{*†1}, Shivanshu Siyanwal^{*‡1}, Abhishek Tiwari^{§1}, Britant^{¶1}, and Savita Kashyap^{||1}

¹Centre for Development of Advanced Computing(C-DAC) Noida, Uttar Pradesh, India - 201307

Abstract

Quantum Machine Learning (QML) presents as a revolutionary approach to weather forecasting by using quantum computing to improve predictive modeling capabilities. In this study, we apply QML models, including Quantum Gated Recurrent Units (QGRUs), Quantum Neural Networks (QNNs), Quantum Long Short-Term Memory (QLSTM), Variational Quantum Circuits (VQCs), and Quantum Support Vector Machines (QSVMs), to analyze meteorological time-series data from the ERA5 dataset. Our methodology includes preprocessing meteorological features, implementing QML architectures for both classification and regression tasks. The results demonstrate that QML models can achieve reasonable accuracy in both prediction and classification tasks, particularly in binary classification. However, challenges such as quantum hardware limitations and noise affect scalability and generalization. This research provides insights into the feasibility of QML for weather prediction, paving the way for further exploration of hybrid quantum-classical frameworks to enhance meteorological forecasting.

1 Introduction

Accurate weather forecasting is essential for various sectors, including agriculture, disaster management, and climate monitoring. Traditional numerical weather prediction models, which rely on solving complex physical equations, often face challenges in computational efficiency and scalability, especially with the increasing volume of meteorological data [1]. Recent advancements in Artificial Intelligence (AI) have significantly improved weather forecasting capabilities by leveraging data-driven approaches. Traditional numerical weather prediction models rely on solving complex physical equations, but AI-based methods can enhance predictive accuracy by learning intricate patterns from large datasets [2]. Studies have shown that deep learning techniques, including convolutional neural networks (CNNs) and recurrent neural networks (RNNs), have been effectively utilized to improve short- and medium-range weather forecasting by capturing nonlinear dependencies in atmospheric data [3]. Notably, AI-driven weather prediction models have demonstrated superior performance compared to conventional approaches, with improvements in forecast accuracy for key meteorological variables such as temperature, wind speed, and precipitation [4].

QML combines quantum computing and machine learning to address the limitations of classical models and improve model performance. QML leverages quantum phenomena such as superposition and entanglement to process complex, high-dimensional data more efficiently [5]. In the context of weather forecasting, QML models have been explored for their potential to improve prediction accuracy and computational speed [6]. For instance, studies have demonstrated the application of parameterized quantum circuits in modeling atmospheric dynamics, achieving accurate reproduction of global stream function dynamics [7].

*These authors contributed equally to this work.

[†]Email: sakhujasaiyam@gmail.com

[‡]Email: shivanshu.siyawal@gmail.com

[§]Email: abhishek@cdac.in

[¶]Email: britant808@gmail.com

^{||}Email: savitakashyap@cdac.in

This study focuses on the application of various QML models—including Quantum Gated Recurrent Units (QGRUs) [8, 9], Quantum Neural Networks (QNNs) [10], Quantum Long Short-Term Memory (QLSTM) [11], Variational Quantum Circuits (VQC) [12], and Quantum Support Vector Machines (QSVMs) [13]—to weather time series data classification and prediction. Utilizing the ERA5 dataset, which offers comprehensive historical weather data, we aim to evaluate the performance of these quantum models in forecasting meteorological parameters. This research seeks to assess the feasibility and potential advantages of QML models in enhancing weather prediction accuracy and classification.

2 Methodology

In this study, we implement quantum-enhanced models for weather prediction using publicly available meteorological datasets. The key components of our methodology include dataset preprocessing and applying QML models for prediction and classification.

2.1 Dataset

This study utilizes the ERA5 reanalysis dataset. It consists of hourly data on single levels from 1940 to the present, provided by the ECMWF through the Copernicus Climate Data Store. ERA5 is the latest generation atmospheric reanalysis of the global climate. The data spans the globe with a 31 km grid resolution and utilizes 137 vertical levels, reaching 80 km in altitude. This allows for hourly estimations of various atmospheric, terrestrial, and marine variables. ERA5 spans from January 1940 to the present, offering a comprehensive and high-resolution record of the Earth’s climate [14, 15]. The data is extracted at 12 PM on the 1st day of each month from 1940 to 2025 for the location Safdarjung Airport (Airports Authority of India), Aurobindo Marg, New Delhi, India. (Latitude: 28.58N, Longitude: 77.20E, Elevation AMSL 805 ft/215 m), which serves as a key meteorological observation site in India. The selected features include various meteorological and surface parameters, such as total precipitation (tp, mm), surface latent heat flux (slhf, J/m^2), surface solar radiation (ssr, J/m^2), surface-thermal radiation (str, J/m^2), surface-sensible heat flux (sshf, J/m^2), surface-downward radiation (ssrd, J/m^2), total sky radiation (tsr, J/m^2), direct solar radiation (fdir, W/m^2), evaporation (e, m), convective precipitation (cp, mm), meridional wind component (mer, m/s), mean total precipitation rate (mtpr, mm/h), 10-meter zonal speed (wind) (u10, m/s), 10-meter meridional speed (wind) (v10, m/s), 2-meter dew point temperature (d2m, K), 2-meter temperature (t2m, K), surface-pressure (sp, Pa), skin temperature (skt, K), 100-meter zonal speed (wind) (u100, m/s), 100-meter meridional speed (wind) (v100, m/s), cloud base height (cbh, m), cloud cover (high) (hcc, %), cloud cover (low) (lcc, %), cloud cover (medium) (mcc, %), cloud cover (total) (tcc, %), convective rain rate (crr, mm/h), vertically integrated water vapor divergence (viwvd, $\text{kg/m}^2/\text{s}$), vertically integrated thermal energy divergence (vithed, $\text{J/m}^2/\text{s}$), and various cloud volume fractions (cvh, cvl, tvh, %). To identify the most relevant features influencing 2-meter temperature (t2m), a correlation-based feature selection technique was employed [16]. Pearson’s correlation coefficient was computed between each feature and t2m to assess their linear relationships.

To identify the most relevant features influencing t2m, a correlation-based feature selection technique was employed. Pearson’s correlation coefficient was computed between each feature and t2m to assess their linear relationships. Table 1 contains the Pearson’s correlation coefficient for some of the features, rest of the values are shown in Figure 1 which shows correlation values of all features with the 2-meter temperature (t2m,K). Features with the highest correlation were selected for further analysis, allowing for the most significant variables to be retained while reducing redundancy and computational complexity.

To ensure consistency and improve the performance of quantum models, we utilized the typical min-max and standard scaling techniques. Standard scaling normalizes data to a zero mean and unit variance, while min-max scaling rescales features to a specific range, usually 0-1, to prevent unit dominance.

Additionally, the target variable ‘t2m’ was converted into two different target representations:

- **Binary classification:** The temperature was categorized into two classes: ‘0’ for values below room temperature (284.53 K - 298 K) and ‘1’ for values above it (298K - 317.59 K).
- **Multi-class classification:** The temperature range was divided into three equal segments: ‘0’ for the lower third (284.53 K - 295.55 K), ‘1’ for the middle third (295.55 K - 306.57 K), and ‘2’ for the upper third of the temperature distribution (306.57 K - 317.59 K).

Table 1: Feature Correlations Values with 2-meter temperature(t2m)

| Feature | skt | tsr | ssrdc | cdir | ssrd | ssr | p54.162 | vithe | fdir | vitoe |
|-------------|-------|------------------|------------------|---------|------------------|------------------|---------|-------|------------------|-------|
| Correlation | 0.972 | 0.803 | 0.783 | 0.778 | 0.766 | 0.759 | 0.689 | 0.678 | 0.668 | 0.542 |
| Units | K | J/m ² | J/m ² | degrees | J/m ² | J/m ² | hPa | K | W/m ² | K |

| Feature | u10 | hcc | mcc | u100 | cbh | v100 | vithed | viwvd | cp | v10 |
|-------------|-------|-------|-------|-------|-------|-------|--------|-------------------|--------|--------|
| Correlation | 0.173 | 0.165 | 0.164 | 0.136 | 0.094 | 0.036 | 0.005 | -0.001 | -0.012 | -0.012 |
| Units | m/s | % | % | m/s | m | m/s | K | kg/m ² | mm | m/s |

| Feature | tp | mtpr | lcc | str | v10n | slhf | e | mer | sshf | sp |
|-------------|--------|--------|--------|------------------|--------|------------------|-------------------|--------|------------------|--------|
| Correlation | -0.025 | -0.025 | -0.103 | -0.133 | -0.179 | -0.531 | -0.531 | -0.531 | -0.561 | -0.806 |
| Units | mm | mm/hr | % | J/m ² | m/s | J/m ² | kg/m ² | m/s | J/m ² | Pa |

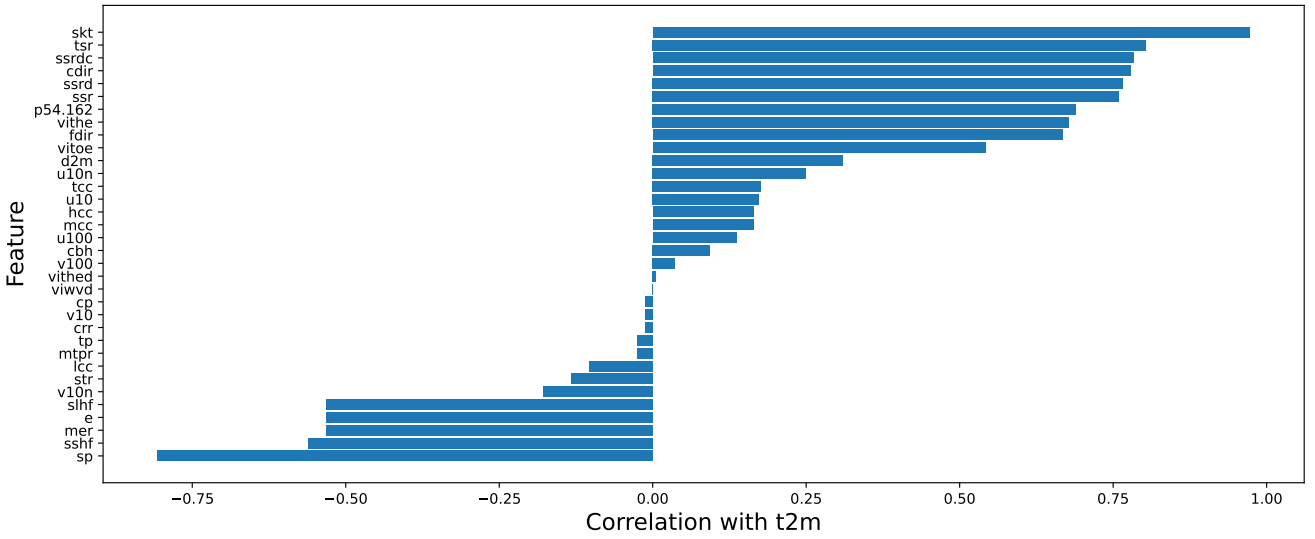


Figure 1: Correlation of each of the dataset features with the 2-meter temperature (t2m,K)

3 Hardware Setup

The experiments in this study were conducted on a high-performance computing system designed to handle quantum machine learning workloads efficiently. The hardware configuration is as follows:

- **CPU:** The system is powered by dual Intel Xeon Gold 6430 processors, each with 32 cores and 64 threads, providing a total of 64 cores and 128 threads. These processors offer a base frequency of 800 MHz and can scale up to 3.4 GHz, ensuring robust parallel processing capabilities essential for pre-processing large-scale meteorological datasets and hybrid quantum-classical computations.
- **GPU:** A NVIDIA RTX A6000 GPU with 48GB of VRAM was utilized for quantum and classical deep learning workloads. This high-memory GPU supports CUDA 12.2 and has a peak power consumption of 300W, making it suitable for running quantum circuit simulations and variational quantum algorithms efficiently.
- **Storage:** The system is equipped with high-capacity storage drives, including:
 - 1.8TB SSD (MR9361-8i by LSI) for fast data access and processing.
 - 3.7TB HDD (MR9361-8i by LSI) for long-term storage and backup of meteorological datasets.

This robust hardware configuration ensured efficient execution of QML models, including **Quantum Gated Recurrent Units (QGRUs)**, **Quantum Neural Networks (QNNs)**, **Quantum Long**

Short-Term Memory (QLSTM), Variational Quantum Circuits (VQC), and Quantum Support Vector Machines (QSVMs). The GPU acceleration was particularly beneficial in training variational quantum circuits, while the multi-core CPU enabled parallelized data pre-processing and hybrid quantum-classical computations [17].

4 Quantum Machine Learning Models

We explore various QML models that extend classical deep learning architectures to quantum-enhanced versions.

4.1 QNN using Ising Layers

Quantum Neural Networks (QNNs) with Ising layers, inspired from [10], utilizes parameterized quantum circuits inspired by the Ising model, which represents interactions between spins in a quantum system. The Ising layers in our QNN architecture consist of multiple entangling gates followed by parameterized single-qubit rotations (RX, RY, RZ). Additionally, a data reuploading strategy, as proposed in [18], is used to encode the input information multiple times across the circuit, allowing the QNN to better capture non-linear relationships in the weather data. The Ising interactions are introduced using entangling blocks, enhancing expressivity while keeping the circuit depth manageable. This architecture ensures that input-dependent quantum correlations are properly modeled, making it suitable for learning patterns in weather forecasting applications. This QNN model has been utilized in both Regression and Classification tasks within Machine Learning, demonstrating its versatility in different predictive scenarios. Fig 2 illustrates the schematics of the QNN circuit with ising layers.

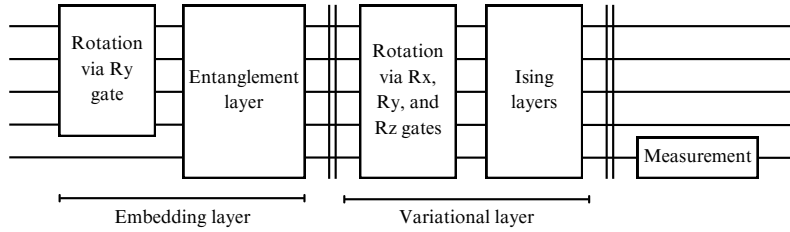


Figure 2: Schematic diagram of the quantum circuit for QNN with ising layers.

4.2 QNN using Strong Entangling Layers

Another QNN variant explored in this study employs Strong Entangling Layers (SELs), inspired by the circuit-centric classifier design [19], as variational layers. These layers introduce deep quantum correlations across qubits, enhancing the expression capacity of the quantum model. Each SEL consists of a series of parameterized single-qubit rotations (RX, RY, RZ) followed by controlled multi-qubit entangling operations. Similar to QNN with ising layers, the data reuploading strategy is used. The strong entangling layers facilitate better feature extraction by increasing the interaction strength between qubits, leading to a richer quantum representation of weather data. Fig 3 shows the architecture of the QNN circuit with SELs.

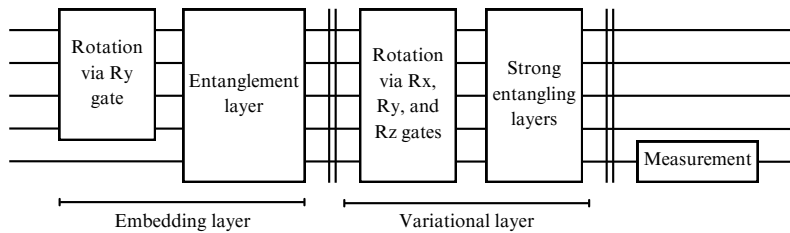


Figure 3: Schematic diagram of the quantum circuit for QNN with Strong entangling layers.

4.3 Quantum Gated Recurrent Units (QGRUs)

The Quantum Gated Recurrent Unit (QGRU) is a quantum adaptation of the classical Gated Recurrent Unit (GRU), engineered to handle complex sequential data such as time-series weather data. Unlike classical GRUs, which rely on classical neural networks, QGRUs employ quantum circuits to encode and process temporal dependencies. The QGRU model described in [8, 9] consists of three Variational Quantum Circuits (VQC1, VQC2, VQC3) embedded within a recurrent unit to control update and reset gates, similar to classical GRUs. These circuits process quantum-encoded input features, and the outputs regulate the hidden state update mechanism. The use of quantum gates for information propagation allows QGRU to capture complex correlations in sequential data efficiently.

In this model, the VQCs are responsible for transforming the inputs and regulating the flow of information through the recurrent unit. The reset gate regulates the amount of past information that is kept, and the update gate controls the blending of past and current inputs. The intermediate output is formed by concatenating the transformed input with the hidden state, which is then processed through another quantum circuit to obtain the candidate hidden state. The final hidden state is updated based on the influence of the update gate. Figure 4 illustrates the QGRUs architecture, with input x , previous hidden state h , and current hidden state H .

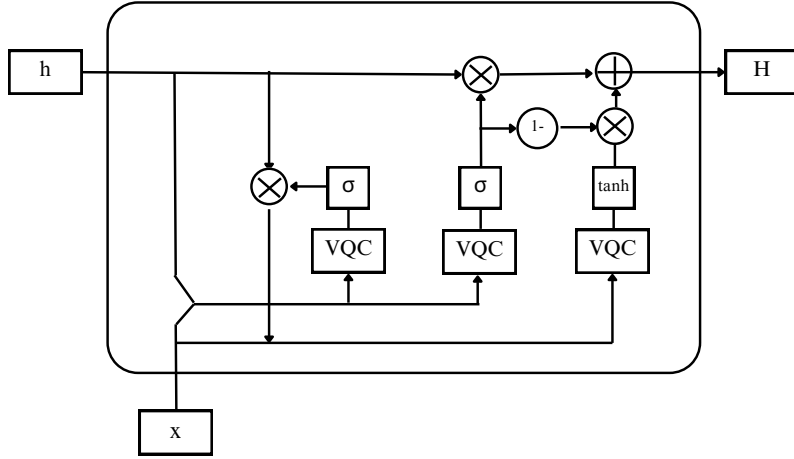


Figure 4: Schematics of the QGRU quantum circuit.

Since the model is designed to predict scalar values, the final hidden state obtained at the last time step is passed through a classical neural network (NN) layer to obtain the output.

4.4 Quantum Long-Short Term Memory (QLSTM)

QLSTM networks enhance classical LSTM architectures by integrating quantum circuits to represent cell and hidden states, using quantum gates to model forget, input, and output gates. This quantum integration enables QLSTMs to capture complex, non-linear spatiotemporal patterns in time-series data, making them particularly effective for weather prediction tasks [11]. Studies have demonstrated that QLSTMs can outperform classical LSTMs in forecasting applications, such as solar power production, by leveraging quantum phenomena like superposition and entanglement to model intricate dependencies in meteorological data [20]. Additionally, studies have explored the Quantum Kernel-Based LSTM (QK-LSTM) to further enhance predictive accuracy and computational efficiency in climate time-series forecasting, embedding classical inputs into high-dimensional quantum feature spaces to capture intricate nonlinear dependencies and temporal dynamics with fewer trainable parameters [21]. Moreover, the Quantum-Train Long Short-Term Memory (QT-LSTM) model has been applied to flood prediction, demonstrating the practicality of quantum machine learning techniques in processing classical data without the need for quantum embedding, thereby improving disaster preparedness and response [22].

The functions σ and \tanh act as activation functions, corresponding to the sigmoid and hyperbolic tangent functions, respectively. The variable $x(t)$ represents the input at time t , while $h(t)$ denotes the hidden state. The cell state is represented by $c(t)$, and $y(t)$ signifies the output. The symbols \otimes and \oplus indicate element-wise multiplication and addition, respectively. The structure of each VQC used in the

model is given in [11] where the data encoding layer consists of H , R_y and R_z gates, with circularly entangled layers and the arbitrary rotation gate $R(\alpha, \beta, \gamma)$ in the variational ansatz layer [11].

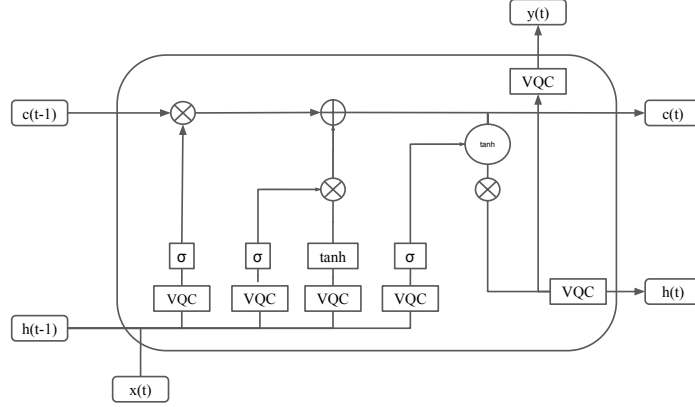


Figure 5: Schematic diagram for QLSTMs.

4.5 Variational Quantum Circuit (VQC)

VQCs are a form of quantum-classical hybrid frameworks in which quantum circuits are optimized through classical algorithms. VQC models utilize parameterized quantum gates to encode and process input data, followed by measurement and classical post-processing. Variational Quantum Circuits (VQCs) have been effectively utilized in both binary and multiclass classification tasks[12]. In binary classification, VQCs are trained to distinguish between two classes by optimizing parameterized quantum circuits to minimize a loss function, thereby enabling the separation of data into two distinct categories [23]. For multiclass classification, VQCs can be extended by employing techniques such as one-versus-all strategies or by designing quantum circuits capable of handling multiple classes simultaneously [24]. These approaches leverage the quantum parallelism inherent in VQCs to process and classify data across multiple categories efficiently [25].

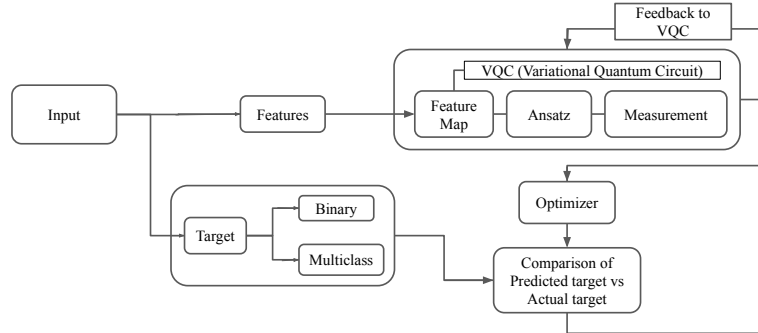


Figure 6: Schematic diagram for VQC (Variational Quantum Circuit).

4.6 Quantum Support Vector Machines (QSVMs)

QSVMs are quantum-enhanced ML models that leverage quantum kernels to perform classification tasks. QSVMs utilize quantum based feature maps to embed input data onto Hilbert space which is generally higher-dimensional, enabling more expressive decision boundaries than classical counterparts. These models rely on quantum kernel estimation to compute inner products in the transformed space, allowing classical support vector machines to achieve improved classification performance [13]. Quantum Support Vector Machines (QSVMs) have been implemented on binary as well as multiclass classification tasks.

In binary classification, QSVMs utilize quantum algorithms to find optimal hyperplanes that separate data into two distinct classes, potentially offering computational advantages over classical SVMs [26]. For multiclass classification, QSVMs can be extended using strategies such as one-against-all or all-pairs approaches, enabling the differentiation among multiple classes [27]. These quantum approaches aim to enhance the efficiency and accuracy of SVMs in complex classification problems [28]. QSVMs have demonstrated potential advantages in complex classification problems, but their practical implementation is constrained by quantum hardware limitations and noise in near-term devices [29].

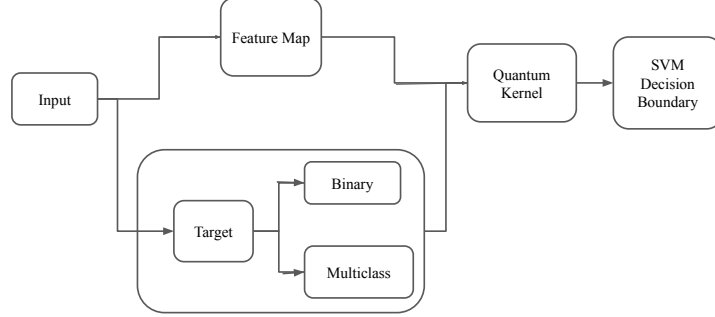


Figure 7: Schematic diagram for QSVM (Quantum Support Vector Machines).

5 Results

The performance of QML models is evaluated based on standard metrics such as accuracy and Mean Squared Error (MSE). For prediction tasks using QGRUs, QNNs, and QLSTMs, the MSE parameter is used as the primary loss function to quantify the deviation between the predicted and actual values. In contrast, for classification tasks involving QNNs, VQCs, and QSVMs, accuracy is used as the key performance metric. The results are compared against their classical counterparts to assess the potential advantages and limitations of quantum models.

5.1 QNN with Ising and Strong Entangling Layers

For both QNN architectures—Ising Layers and Strong Entangling Layers—we utilized a common data preprocessing pipeline. Features were selected based on correlation thresholds, with the top three correlated features chosen for the Ising Layer model (± 0.8 threshold) and the top four for the Strong Entangling Layer model (± 0.78 threshold). Normalization was applied in both cases.

Both models were employed for regression and classification tasks. In regression, the target variable was used as is.

To enhance performance, we implemented the data reuploading strategy in both models. Our experimental results demonstrate that this approach improves model accuracy across tasks.

Table 2 shows the results for binary classification and multi-class classification using QNN with ising layer as variational layer, while Fig. 8a shows the prediction results. Table 3 shows the results for binary classification and multi-class classification using QNN with strong entangling layer as variational layer, while Fig. 8b shows the prediction results. For the QNN Ising model, the classical neural network achieves a test loss of 4.14, whereas the quantum neural network achieves a lower test loss of 3.86 with the same number of trainable parameters (21). In contrast, for the Quantum Strong Entangling Layer model, the classical neural network attains a test loss of 2.58, while the quantum neural network yields a slightly higher test loss of 2.95 with an equal number of trainable parameters (48).

Table 2: Summary of comparative classification Results for QNN - Ising

| Model | Metric | Binary Classification | Multi-Class Classification |
|--------------|-------------------|-----------------------|----------------------------|
| QNN-Ising | Training accuracy | 0.9501 | 0.8670 |
| QNN-Ising | Test accuracy | 0.9565 | 0.8495 |
| Classical NN | Training accuracy | 0.9397 | 0.8850 |
| Classical NN | Test accuracy | 0.9362 | 0.8762 |

Table 3: Summary of comparative classification Results for QNN - Strong Entangling Layer (SEs)

| Model | Metric | Binary Classification | Multi-Class Classification |
|--------------|-------------------|-----------------------|----------------------------|
| QNN-SEL | Training accuracy | 0.9799 | 0.9002 |
| QNN-SEL | Test accuracy | 0.9653 | 0.8762 |
| Classical NN | Training accuracy | 0.9598 | 0.9030 |
| Classical NN | Test accuracy | 0.9556 | 0.8862 |

5.2 Quantum Gated Recurrent Units (QGRUs)

After the data is preprocessed, from all the features, we took the most correlated features, namely, Surface Solar Radiation Downward Clear-Sky (ssrdc), Top Net Solar Radiation (tsr), Surface Pressure (sp), and Skin Temperature (skt), with the target feature being Temperature Above 2m Surface (t2m). The training and test loss values after 20 epochs for the QGRU model were 2.25 and 2.65, respectively. Fig. 9a shows the prediction results of the QGRU model. Notably, the number of trainable parameters for the QGRU model is significantly lower compared to its classical counterpart, with 16 neurons and 1 hidden layer highlighting the potential of quantum models in reducing parameter complexity while maintaining performance. Table 4 shows the comparison of trainable parameters in classical and quantum version of GRUs.

5.3 Quantum Long-Short Term Memory (QLSTM)

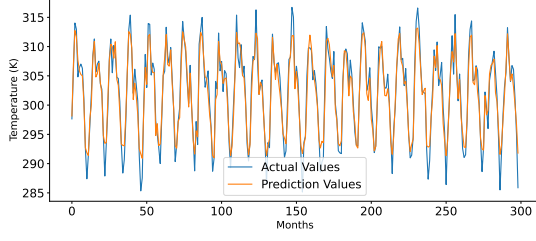
For implementing QLSTMs, we used quantum-classical hybrid framework, where quantum circuits process sequential inputs and interact with classical optimizers. The QLSTM model employs a total of six variational quantum circuits (VQCs) to encode and manipulate information at each time step, allowing for quantum-enhanced temporal modeling. Unlike classical LSTMs, where memory units rely on weighted summations and activation functions, QLSTM leverages quantum entanglement and superposition for state evolution as inspired from the original work done by Samuel Yen-Chi Chen et al. [11]. Training QLSTM involves variational parameter tuning using gradient-based method Autograd algorithm. The model is initialized with a learning rate of 0.01 with 16 hidden units, the overall model uses 4 qubits corresponding to the top 4 features in the dataset. The final QLSTM train and test loss values after 50 epochs are 0.0456 and 0.0536, respectively. Figure 9b shows the prediction results of the QLSTM model. Notably, the number of trainable parameters for the QLSTM model is significantly lower compared to its classical counterpart, with 8 neurons and 1 hidden layer highlighting the potential of quantum models in reducing parameter complexity while maintaining performance. Table 4 shows the comparison of trainable parameters in classical and quantum version of LSTMs.

| Model | Trainable Parameters (Classical) | Trainable Parameters (Quantum) |
|-------|----------------------------------|--------------------------------|
| GRUs | 1073 | 164 |
| LSTMs | 457 | 181 |

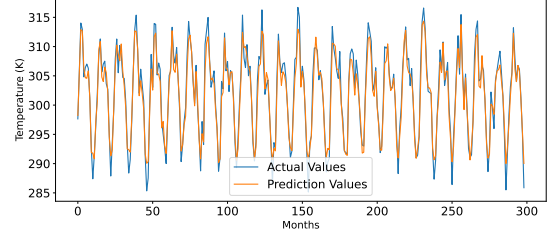
Table 4: Comparison of trainable parameters in classical and quantum LSTMs and GRUs.

5.4 Variational Quantum Circuit (VQC)

VQCs in our study were constructed using the ZZ Feature Map with 1 layer (linear entanglement) and Real Amplitudes Ansatz with 3 layers (linear entanglement). The models have been applied over both

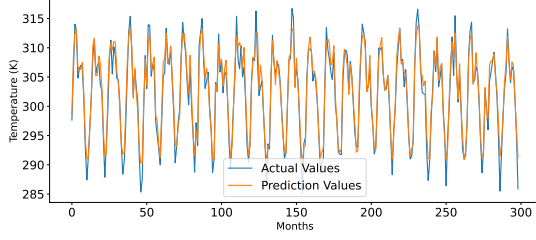


(a) Temperature prediction over test dataset using QNN Ising Model.

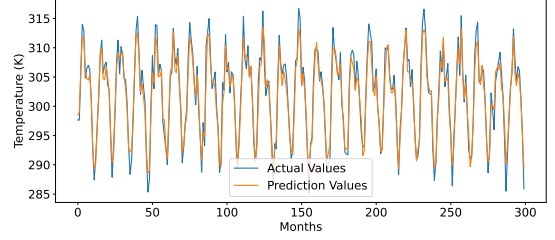


(b) Temperature prediction over test dataset using QNN Strong Entangling Layer Model.

Figure 8: Comparison of Ising and Strong Entangling Layer model results.



(a) Temperature prediction over the test dataset using QGRU.



(b) Temperature prediction over the test dataset using QLSTM.

Figure 9: Comparison of QGRU and QLSTM temperature predictions.

binary and multi-classification problems. Optimization was performed using the COBYLA optimizer for 150 iterations. The results are mentioned in the table 5, as apparent, accuracies for multiclass (0.78, 0.79) is overall lower compared to binary (0.93, 0.95).

Table 5: Summary of classification accuracy results (VQC)

| Model | Metric | Binary Classification | Multi-Class Classification |
|-------|-------------------|-----------------------|----------------------------|
| VQC | Training accuracy | 0.9354 | 0.7842 |
| VQC | Test accuracy | 0.9522 | 0.7951 |
| SVC | Training accuracy | 0.9667 | 0.9155 |
| SVC | Test accuracy | 0.9665 | 0.9230 |

5.5 Quantum Support Vector Machines (QSVM)

QSVMs are also applied on both the binary and multi classification problems as mentioned above, we have used the Z feature map with 4 top features and 1 repetitions alongwith a Quantum Kernel based on fidelity. The input data is preprocessed with the min-max scaling. The results are mentioned in Table 6, As is apparent from the results, accuracies for multiclass (0.88, 0.86) are much lower compared to that of binary (0.95, 0.96).

6 Conclusion and Future Works

This study utilizes the ERA5 reanalysis dataset to test the ability of various QML models, including QGRUs, QNNs, QLSTMs, VQCs, and QSVMs. Our results indicate that these quantum models can effectively capture patterns in meteorological data and, in certain cases, achieve competitive accuracy compared to classical machine learning methods.

The experiments demonstrated that QML models offer potential advantages in handling high dimensional weather data owing to their capacity of processing information in a quantum-parallel manner. QGRUs and QLSTMs, in particular, showcased promising performance in time-series forecasting, while

Table 6: Summary of classification accuracy results (QSVM)

| Model | Metric | Binary Classification | Multi-Class Classification |
|-------|-------------------|-----------------------|----------------------------|
| QSVM | Training accuracy | 0.9531 | 0.8808 |
| QSVM | Test accuracy | 0.9584 | 0.8628 |
| SVC | Training accuracy | 0.9667 | 0.9155 |
| SVC | Test accuracy | 0.9665 | 0.9230 |

QNN-based models with Ising and Strong Entangling Layers performed well in both regression and classification tasks. Furthermore, VQC and QSVM models exhibited effective classification capabilities, particularly in binary classification scenarios. However, multiclass classification remains a challenge due to quantum circuit limitations.

Despite these advantages, several obstacles must be addressed before practical implementation. Challenges such as limited qubit availability, noise in quantum hardware, and computational constraints continue to impact the feasibility of QML models in real-world weather forecasting applications. Future work should focus on improving the scalability of quantum models, optimizing hybrid quantum-classical architectures, and leveraging error-mitigation techniques to enhance prediction accuracy and reliability.

In conclusion, our study provides insights into the application of QML models for weather prediction, highlighting both their potential and existing limitations. Continued developments in quantum algorithms and quantum hardware are bound to lead a crucial role for determining the practical applications of QML in meteorological domain.

In future work, we plan to incorporate additional features for weather forecasting and increase the number of data points to enhance model performance. This expansion will lead to an increase in the number of qubits and circuit depth required for the quantum models. Optimizing quantum circuit architectures and exploring efficient encoding schemes will be crucial to managing these complexities while maintaining computational feasibility.

References

- [1] J. A. Brotzge, D. Berchhoff, D. L. Carlis, F. H. Carr, R. H. Carr, J. J. Gerth, B. D. Gross, T. M. Hamill, S. E. Haupt, N. Jacobs, A. McGovern, D. J. Stensrud, G. Szatkowski, I. Szunyogh, and X. Wang, “Challenges and opportunities in numerical weather prediction,” *Bulletin of the American Meteorological Society*, vol. 104, no. 3, pp. E698 – E705, 2023.
- [2] B. Bochenek and Z. Ustrnul, “Machine learning in weather prediction and climate analyses—applications and perspectives,” *Atmosphere*, vol. 13, no. 2, 2022.
- [3] L. Han, M. Chen, K. Chen, H. Chen, Y. Zhang, B. Lu, L. Song, and R. Qin, “A deep learning method for bias correction of ecmwf 24–240 h forecasts,” *Advances in Atmospheric Sciences*, vol. 38, pp. 1444 – 1459, 2021.
- [4] J. Frnda, M. Durica, J. Rozhon, M. Vojteková, J. Nedoma, and R. Martínek, “Ecmwf short-term prediction accuracy improvement by deep learning,” *Scientific Reports*, vol. 12, 2022.
- [5] J. Biamonte, P. Wittek, N. Pancotti, P. Rebentrost, N. Wiebe, and S. Lloyd, “Quantum machine learning,” *Nature*, vol. 549, p. 195–202, Sept. 2017.
- [6] B. Surendiran, K. Dhanasekaran, and A. Tamizhselvi, “A study on quantum machine learning for accurate and efficient weather prediction,” in *2022 Sixth International Conference on I-SMAC (IoT in Social, Mobile, Analytics and Cloud) (I-SMAC)*, pp. 534–537, 2022.
- [7] B. Jaderberg, A. A. Gentile, A. Ghosh, V. E. Elfving, C. Jones, D. Vodola, J. Manobianco, and H. Weiss, “Potential of quantum scientific machine learning applied to weather modelling,” 2024.
- [8] S. Y.-C. Chen, D. Fry, A. Deshmukh, V. Rastunkov, and C. Stefanski, “Reservoir computing via quantum recurrent neural networks,” *arXiv preprint arXiv:2211.02612*, 2022.

- [9] Y. Chen and A. Khaliq, “Quantum recurrent neural networks: Predicting the dynamics of oscillatory and chaotic systems,” *Algorithms*, vol. 17, no. 4, p. 163, 2024.
- [10] D. Emmanoulopoulos and S. Dimoska, “Quantum machine learning in finance: Time series forecasting,” *arXiv preprint arXiv:2202.00599*, 2022.
- [11] S. Y.-C. Chen, S. Yoo, and Y.-L. L. Fang, “Quantum long short-term memory,” 2020.
- [12] M. Cerezo, A. Arrasmith, R. Babbush, S. C. Benjamin, S. Endo, K. Fujii, J. R. McClean, K. Mitarai, X. Yuan, L. Cincio, and P. J. Coles, “Variational quantum algorithms,” *Nature Reviews Physics*, vol. 3, p. 625–644, Aug. 2021.
- [13] P. Rebentrost, M. Mohseni, and S. Lloyd, “Quantum support vector machine for big data classification,” *Phys. Rev. Lett.*, vol. 113, p. 130503, Sep 2014.
- [14] H. Hersbach, B. Bell, P. Berrisford, S. Hirahara, A. Horányi, J. Muñoz-Sabater, J. Nicolas, C. Peubey, R. Radu, D. Schepers, A. Simmons, C. Soci, S. Abdalla, X. Abellan, G. Balsamo, P. Bechtold, G. Biavati, J. Bidlot, M. Bonavita, G. De Chiara, P. Dahlgren, D. Dee, M. Diamantakis, R. Dragani, J. Flemming, R. Forbes, M. Fuentes, A. Geer, L. Haimberger, S. Healy, R. J. Hogan, E. Hólm, M. Janisková, S. Keeley, P. Laloyaux, P. Lopez, C. Lupu, G. Radnoti, P. de Rosnay, I. Rozum, F. Vamborg, S. Villaume, and J.-N. Thépaut, “The era5 global reanalysis,” *Quarterly Journal of the Royal Meteorological Society*, vol. 146, no. 730, pp. 1999–2049, 2020.
- [15] J. Muñoz Sabater, E. Dutra, A. Agustí-Panareda, C. Albergel, G. Arduini, G. Balsamo, S. Boussetta, M. Choulga, S. Harrigan, H. Hersbach, B. Martens, D. G. Miralles, M. Piles, N. J. Rodríguez-Fernández, E. Zsoter, C. Buontempo, and J.-N. Thépaut, “Era5-land: a state-of-the-art global reanalysis dataset for land applications,” *Earth System Science Data*, vol. 13, no. 9, pp. 4349–4383, 2021.
- [16] P. Sedgwick, “Pearson’s correlation coefficient,” *Bmj*, vol. 345, 2012.
- [17] NVIDIA, P. Vingelmann, and F. H. Fitzek, “Cuda, release: 10.2.89,” 2020.
- [18] A. Pérez-Salinas, A. Cervera-Lierta, E. Gil-Fuster, and J. I. Latorre, “Data re-uploading for a universal quantum classifier,” *Quantum*, vol. 4, p. 226, 2020.
- [19] M. Schuld, A. Bocharov, K. M. Svore, and N. Wiebe, “Circuit-centric quantum classifiers,” *Physical Review A*, vol. 101, no. 3, p. 032308, 2020.
- [20] S. Z. Khan, N. Muzammil, S. Ghafoor, H. Khan, S. M. H. Zaidi, A. J. Aljohani, and I. Aziz, “Quantum long short-term memory (qlstm) vs. classical lstm in time series forecasting: a comparative study in solar power forecasting,” *Frontiers in Physics*, vol. 12, 2024.
- [21] Y.-C. Hsu, N.-Y. Chen, T.-Y. Li, Po-Heng, Lee, and K.-C. Chen, “Quantum kernel-based long short-term memory for climate time-series forecasting,” 2024.
- [22] C.-H. A. Lin, C.-Y. Liu, and K.-C. Chen, “Quantum-train long short-term memory: Application on flood prediction problem,” 2024.
- [23] M. T. Kakız, E. Güler, T. Çavdar, and B. Şanal, “Binary classification with variational quantum circuit,” in *2023 Innovations in Intelligent Systems and Applications Conference (ASYU)*, pp. 1–7, 2023.
- [24] J. Wu, T. Hu, and Q. Li, “More: Measurement and correlation based variational quantum circuit for multi-classification,” 2023.
- [25] I. Piatrenka and M. Rusek, “Quantum variational multi-class classifier for the iris data set,” in *Computational Science – ICCS 2022* (D. Groen, C. de Mulatier, M. Paszynski, V. V. Krzhizhanovskaya, J. J. Dongarra, and P. M. A. Sloot, eds.), (Cham), pp. 247–260, Springer International Publishing, 2022.

- [26] T. Suzuki, T. Hasebe, and T. Miyazaki, “Quantum support vector machines for classification and regression on a trapped-ion quantum computer,” *Quantum Machine Intelligence*, vol. 6, 05 2024.
- [27] A. K. Bishwas, A. Mani, and V. Palade, “Big data classification with quantum multiclass svm and quantum one-against-all approach,” in *2016 2nd International Conference on Contemporary Computing and Informatics (IC3I)*, pp. 875–880, 2016.
- [28] A. K. Bishwas, A. Mani, and V. Palade, “An all-pair quantum svm approach for big data multiclass classification,” *Quantum Information Processing*, vol. 17, Sept. 2018.
- [29] Z. Li, X. Liu, N. Xu, and J. Du, “Experimental realization of a quantum support vector machine,” *Phys. Rev. Lett.*, vol. 114, p. 140504, Apr 2015.